

SCIENTIFIC REPORTS



OPEN

Accelerated phosphorus recovery from aqueous solution onto decorated sewage sludge carbon

Lingjun Kong^{1,2}, Xingliang Hu¹, Ziyang Xie¹, Xinyong Ren¹, Jianyou Long¹, Minhua Su¹, Zenghui Diao³, Diyun Chen¹, Kaimin Shih² & Li'an Hou¹

In search of efficient phosphorus resource recovery and pollution remediation should be highly concerned due to the view of phosphorus nonrenewable and eutrophication. This work presented a new insight into conversion of sewage sludge into favorable carbonaceous adsorbent for accelerated removing and recovering phosphorus from aqueous solution, what addressed the issues of phosphorus recovery and pollution remediation as well as sludge disposal. Ca and water hyacinth were evolved to decorate sludge derived carbon. Effect of mass ratio of sludge, water hyacinth and calcium carbonate on the morphologies and adsorption kinetics was investigated. The adsorbents (SW-Ca-112) resulted from sludge in the presence of water hyacinth and CaCO₃ in a mass ratio of 1:1:2 had the highest adsorption capacity of 49.50 mg/g P and adsorption rate. Decoration of Ca favored adsorption ability and the presence of water hyacinth accelerated the adsorption rate due to the enhanced porosity. Formation of acicular Ca₅(PO₄)₃OH nanoparticles contributed to the favorable adsorption process. Thus, the contribution of decorated Ca and water hyacinth to the adsorption ability and rate to phosphorus was understood, providing important information on resource utilization of sewage sludge as efficient adsorbent for immobilizing phosphorus from aqueous solution.

Phosphorus (P), as one of raw materials in fertilizer production, is urgently demand in these days. However, the P resource is non-renewable¹. It is estimated that phosphate rock lasts for only 100 years². Unfortunately, high level of P was founded in some surface water bodies in China due to discharge of P carried by domestic and industrial sewers. The severe runoff of excessive P triggers eutrophication. Resource of P from P pollution water body follows the point view of resource cycle and sustainable, what is prospective. In the past decades, various adsorbents from carbon to minerals were designed to extract P from aqueous solution³⁻⁹. It is promise to design environmental friendly materials from waste.

Sewage sludge, as an inevitable byproduct generated from sewage treatment, is produced in a large amount around the world as the rapid development of urbanization¹⁰. Reuse of waste sludge to product is compliant for life cycle assessment studies¹¹. It is reviewed from literatures that sludge substances and its derived carbonaceous were widely applied in removing organic compounds, heavy metals¹²⁻¹⁴. Carbonization of sludge to produce low-cost sludge carbon has emerged as a sustainable strategy for sewage sludge management¹⁵, because this strategy takes the advantages in not only reducing sewage sludge volume but also converting solid waste into adsorbents^{13,16-19} and catalysts²⁰⁻²⁴ for environmental pollution remediation. Extraction of P by sewage sludge and its ash was paid more attention²⁵. Recently, Ca-decorated sludge biochar was prepared for phosphorus pollution remediation, in which the sludge biochar could be acted as a carrier and Ca could react with phosphorus by complexation²⁶.

However, the surface area is limited comparing to the activated carbon obtained from coal and agriculture waste due to their high mineral contents^{27,28}. Addition of carbon rich biomass to sludge could address the above issue²⁹. Wu *et al.* reported that the surface area could be increased from 287 to 591 m²/g, further increased the microporosity from 5% to 48% due to the addition of biomass³⁰.

¹Guangdong Provincial Key Laboratory of Radioactive Contamination Control and Resources, School of Environmental Science and Engineering, Guangzhou University, Guangzhou, 510006, P.R. China. ²Department of Civil Engineering, The University of Hong Kong, Pokfulam Road, Hong Kong, P.R. China. ³School of Environmental Science and Engineering, Zhongkai University of Agriculture and Engineering, Guangzhou, 510225, China. Correspondence and requests for materials should be addressed to L.K. (email: kongljun@gzhu.edu.cn)

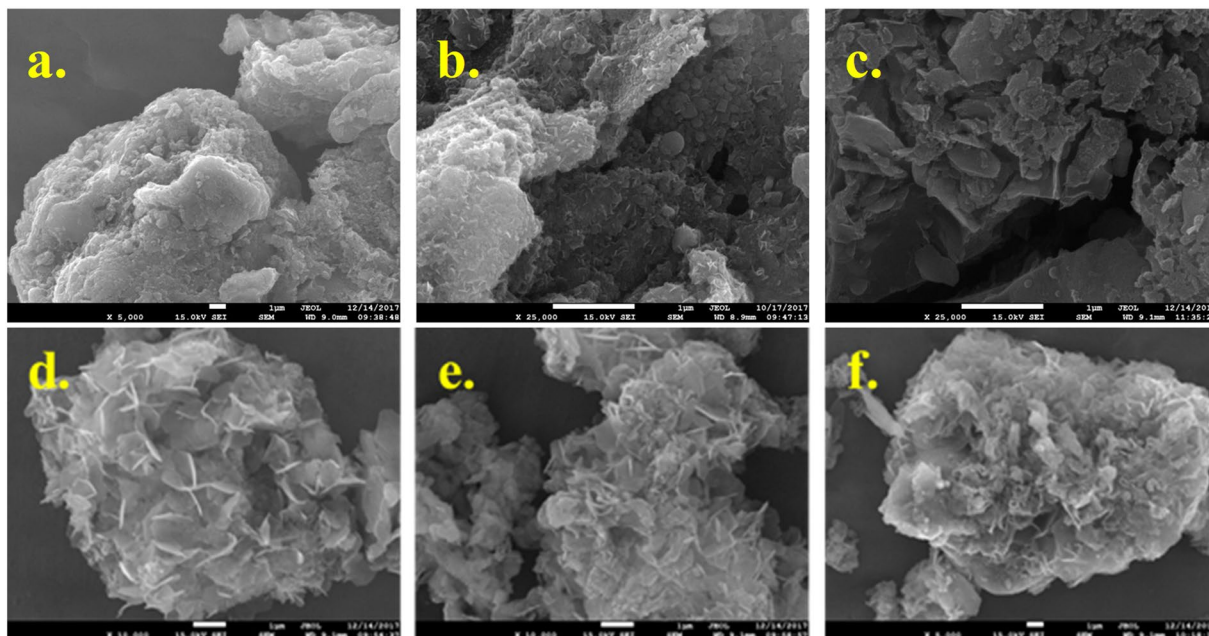


Figure 1. SEM morphologies of the sludge derived biochars: (a) sludge char (S), (b) S-Ca-11, (c) S-W-11, (d) SW-Ca-112, (e) SW-Ca-325, (f) SW-Ca-415.

Water hyacinth (W) is a water weed in several water bodies (e.g., lakers, rivers, canals) around the world³¹. This plant grows rapidly and can completely cover water bodies, causing difficulty in navigation and depletion of nutrients and dissolved oxygen that are essential for aquatic life. These effects have negative impact on the ecological environment, human health, and economic development³². Treatment of water hyacinth has become a serious environmental problem in many parts of the world. Therefore, water hyacinth is considered to be a suitable and an easily available biomass³³. Considering its high volatile content, utilization of water hyacinth for preparing biochar with loose structure could be considered as one of the most economical and environmental friendly ways for treatment and final disposal of water hyacinth.

In this study, another kind of sewage sludge was resourced as carbonaceous adsorbent for removing and recovering phosphorus, in which it was decorated by Ca, and water hyacinth was added to accelerate its adsorption rate. Herein, water hyacinth was mixed with sewage sludge in varied mass ratio, being carbonized at 800 °C for preparing efficient adsorbent. Batch adsorption experiments were conducted to investigate the adsorption behavior while XRD and SEM techniques were conducted to further understand the adsorption mechanism by morphology and phase analysis. This work gives a new insight into understanding the effect of Ca and water hyacinth decoration on the adsorption capacity and rate to phosphorus from aqueous solution, providing a new view in sludge resource utilization as well as phosphorus removal and recovery.

Results and Discussion

Morphology of the biochar. Figure 1 presented the micro-morphology of the resulted biochars. Obviously, the particles were agglomerated and tight after being carbonized. Interestingly, some small nanoflakes were observed after addition of CaCO_3 as shown in Fig. 1(b) comparing to the samples derived from sludge as shown in Fig. 1(a). However, nanoflake was not observed, but many cracks were observed for biochar in the presence of water hyacinth as shown in Fig. 1(c). Amazingly, many cracks and flakes were observed after adding water hyacinth and CaCO_3 as shown in Fig. 1(d–f). These cracks fabricated due to the addition of water hyacinth and CaCO_3 could increase the porosity of biochar³⁰. The nanoflake was assigned to the Ca derived material. It is different from our previous results that nano-rods were observed in the presence of CaCO_3 ²⁶. The difference may be due to the interaction between CaCO_3 and sludge, what could be confirmed in the future. Also, we can observe that the nano-flake structure was different from the ratio of sludge to water hyacinth. The nanoflakes were distinct for the resulted samples in a higher mass ratio of hyacinth to sludge as shown in Fig. 1(d). With the decrease in mass ratio of water hyacinth to sludge, the agglomeration of nanoparticle was observed as shown in Fig. 1(e,f). Because volatile content of water hyacinth was 77.47%, a lot of volatile was decomposed and emitted after carbonization. Thus, the decomposition of volatiles led to formation of many cracks and increase in porosity. This result suggested that the presence of water hyacinth increased the porosity of biochar, further providing considerable channels favoring phosphorus adsorption.

Adsorption behaviors. Figure 2 presented the adsorption amounts of phosphorus as a function of contact time. Clearly, the adsorption capacity of sludge char (S) is very low, which is not higher than 5 mg/g. Interestingly, the adsorption capacity highly increased to almost 50 mg/g in the presence of calcium decoration. Adsorption of phosphorus on S could be neglectful, while the addition of CaCO_3 highly favored phosphorus adsorption, meaning that the favorable adsorption abilities of SW-Ca-112 and S-Ca-11 to phosphorus were ascribed to the

Samples	Pseudo-first-order model			Pseudo-second-order model		
	q_e (mg/g)	k_1 (min^{-1})	R^2	q_e (mg/g)	k_2 (g/(mg·min))	R^2
S-Ca-11	17.8678	0.01148	0.8446	49.9500	0.0036	0.9983
SW-Ca-112	17.9382	0.03094	0.9454	49.5050	0.0083	0.9999

Table 1. Adsorption kinetic parameters of phosphorus onto sludge derived adsorbents in the presence of water hyacinth and Ca.

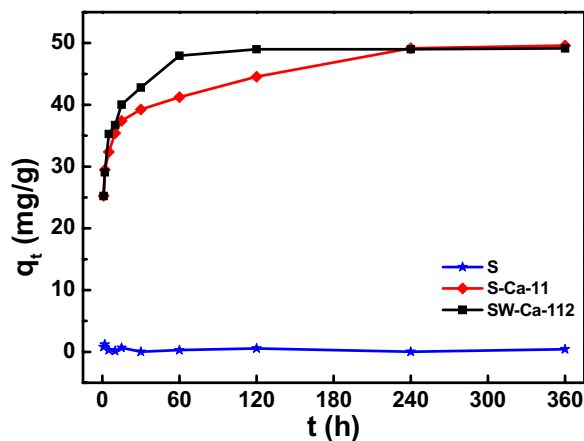


Figure 2. Adsorption capacities of sludge derived char as a function of contact time.

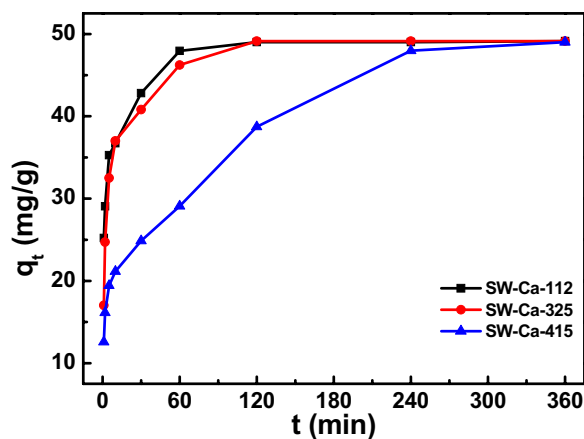


Figure 3. Effect of water hyacinth contents on adsorption capacities as a function of contact time.

decorated calcium. It also can be seen that the adsorption capacities were CaCO_3 dependent since S-Ca-11 had similar adsorption capacity to SW-Ca-112. Interestingly, the adsorption kinetic process is quite different due to the addition of water hyacinth.

Adsorption kinetic models described in Eqs (2) and (3) were conducted to investigate the kinetic parameters, what were listed in Table 1. Clearly, the pseudo-second-order model fitted well to the adsorption data considering the high correlation coefficients as shown in Table 1. In addition, it can be seen from Table 1 that the adsorption rate of SW-Ca-112 highly increased to 0.0083 in the presence of water hyacinth. It was 2.3 times comparing to that of S-Ca-11 in the absence of water hyacinth, indicating the accelerated adsorption kinetic rate. The increased adsorption rate was agreement with the formed cracks and flakes, suggesting that the cracks and flakes fabricated from decomposition of water hyacinth favored the preferable adsorption rate.

To further investigate the effect of addition of water hyacinth on the adsorption behavior, mass content of CaCO_3 was fixed to 50%, and the adsorption capacities of adsorbents in varied mass ratio of sludge to water hyacinth were presented in Fig. 3. They had the same equilibrium adsorption capacities of about 49.50 mg/g P, but the reaction time to equilibrium was different. SW-Ca-112, SW-Ca-325 had similar equilibrium time of 120 min because the mass ratio of sludge to water hyacinth was similar, while SW-Ca-415 had a longer equilibrium time of 240 min due to the relative low water hyacinth content. Also, as can be seen from Fig. 1(f), the cracks of

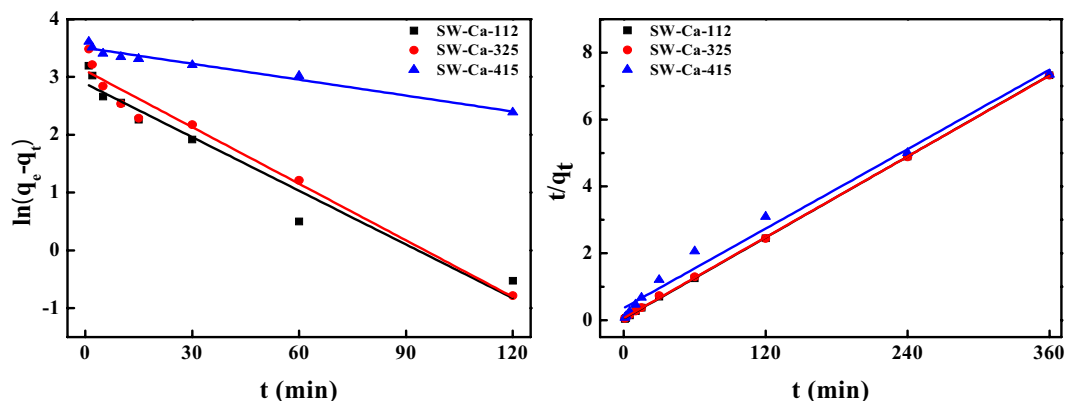


Figure 4. Linear fitted adsorption kinetics of phosphorus on the SW-Ca with varied mass ratio: (a) pseudo-first-order model and (b) pseudo-second-order model.

Samples	Pseudo-first-order model			Pseudo-second-order model		
	q_e (mg/g)	k_1 (min^{-1})	R^2	q_e (mg/g)	k_2 (g/(mg·min))	R^2
SW-Ca-112	17.9382	0.0309	0.9454	49.5050	0.0083	0.9999
SW-Ca-325	22.4502	0.0326	0.9656	49.6771	0.0062	0.9998
SW-Ca-415	33.2908	0.0092	0.9672	50.5306	0.0011	0.9852

Table 2. Adsorption kinetic parameters of phosphorus onto SW-Ca derived adsorbents with varied water hyacinth and sludge content.

SW-Ca-415 were not as distinct as those of SW-Ca-112 and SW-Ca-325. Therefore, the shorter time to equilibrium of SW-Ca-112 and SW-Ca-325 than that of SW-Ca-415 was concluded from the fabricated cracks by decomposition of water hyacinth. The presence of water hyacinth highly decreases the time to equilibrium. In addition, it is not hard to understand that the adsorption capacities are determined by the decorated Ca as shown in our previous study³⁴.

Two widely used pseudo-first-order and pseudo-second-order models were presented to fit the above experimental data to evaluate the adsorption rate, and the nonlinear fitted technique was applied to estimate the kinetic parameters³⁵. However, the nonlinear optimization was not fit for the experimental data adequately (Fig. S1). Linear optimization techniques were applied to estimate the experimental results and corresponding parameters were listed in Fig. 4 and Table 2. Considering the correlation coefficients shown in Table 2, adsorption of P onto SW-Ca-112, SW-Ca-325 fitted well by the pseudo-second-order model. In addition, the fitted equilibrium adsorption capacities of 49.50 and 49.68 mg/g onto SW-Ca-112, SW-Ca-325 were quite agreement with the experimental adsorption capacities. Since the pseudo-second-order model is based on the assumption that adsorption of P onto adsorbent involves the chemical reaction between PO_4^{3-} and Ca, as reported by Mitrogiannis *et al.*³⁶, indicating a chemisorptions-dominated process. Also, the adsorption capacity to P is higher than the previous results^{36–39}. Importantly, the fitted adsorption rate calculated from pseudo-second-order model for SW-Ca-112 was higher than that for SW-Ca-325 due to higher content of water hyacinth. In addition, the SW-Ca-415 had quite low adsorption rate due to the low content of water hyacinth. These results were quite agreement with the fabricated cracks of SW-Ca-112, SW-Ca-325 and SW-Ca-415 as shown in Fig. 1. Thus, these results all confirmed that the presence of water hyacinth could accelerate the adsorption rate due to fabrication of favorable cracks.

Figure 5 showed that the adsorption capacity of P depended on the CaCO_3 content. Pseudo-first-order and pseudo-second-order models were performed to fit the experiment data. The fitted parameters were listed in Table 3. Clearly, pseudo-second-order model was better than pseudo-first-order model to fit the adsorption experiments as indicated by the favorable correlation coefficients. In addition, the calculated equilibrium adsorption capacities for SW-Ca-112, SW-Ca-221 and SW-Ca-441 were quite agreement with the experimental data. The SW-Ca-441 with the lowest CaCO_3 content had the lowest adsorption capacity to P. This result confirmed that the favorable adsorption capacity to P was determined by the chemical reaction of P with Ca. In addition, the adsorption rates calculated from pseudo-second-order model were agreement with the CaCO_3 ratio. The higher CaCO_3 ratio, the higher adsorption rate was. Thus, it is easy to conclude that the decorated Ca plays a key role in influencing the adsorption capacity.

Characterization of adsorption products. The products after adsorption of P were characterized by SEM analysis as shown in Fig. 6. Comparing to the samples before adsorption, nanoparticles in acicular was observed on the nanoflakes. Especially, these nanoparticles were well dispersed onto the well dispersed nanoflakes of SW-Ca-112 (as shown in Fig. 6(a)). For the other SW-Ca-325 and SW-Ca-415, nanoparticles were also

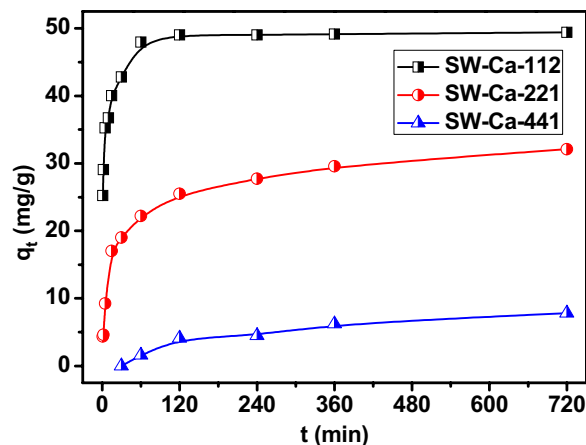


Figure 5. Effect of CaCO_3 contents on the P adsorption capacity.

Samples	Pseudo-first-order model			Pseudo-second-order model		
	q_e (mg/g)	k_1 (min^{-1})	R^2	q_e (mg/g)	k_2 ($\text{g}/(\text{mg}\cdot\text{min})$)	R^2
SW-Ca-112	18.2910	2.0467	0.9620	49.1642	0.7410	0.9999
SW-Ca-221	23.8566	0.6490	0.8303	33.3222	0.07340	0.9989
SW-Ca-441	10.9412	0.4155	0.9994	10.6168	0.0204	0.9864

Table 3. Adsorption kinetic parameters of phosphorus onto SW-Ca derived adsorbents with varied Ca content.

observed on the surface of nanoflakes. The observed nanoparticles could be ascribed to the crystal products after reaction of P with Ca.

XRD analysis of the adsorbents before and after phosphorus adsorption was conducted in Fig. 7 to understand the phase of the crystal nanoparticles after adsorption. The diffraction peaks assigned to CaCO_3 and $\text{Ca}(\text{OH})_2$ were observed in the presence of CaCO_3 . The presented $\text{Ca}(\text{OH})_2$ was due to the decomposition of CaCO_3 into CaO and CO_2 , further the CaO can react with the water during adsorption to form $\text{Ca}(\text{OH})_2$ ²⁶. Besides, diffraction peaks located at 33.2° , being assigned to $\text{Ca}_5(\text{PO}_4)_3\text{OH}$, were both observed for adsorbents before and after P adsorption. The presence of $\text{Ca}_5(\text{PO}_4)_3\text{OH}$ before P adsorption was due to the initial P content in these sludge derived chars were about 1.17 to 1.71% (Table S2). And $\text{Ca}_5(\text{PO}_4)_3\text{OH}$ crystal was also observed after P adsorption, but mass content of P after adsorption increased to 8.46% (Table 4). The increase in the P content indicated favorable P adsorption, and the $\text{Ca}_5(\text{PO}_4)_3\text{OH}$ crystal was the fate of P after adsorption.

Conclusion

Sewage sludge was successfully converted into carbonaceous adsorbent for removing and recovering phosphorus from aqueous solution, in which decorated Ca favored adsorption capacity while added water hyacinth accelerated the adsorption rate. Nanoflakes were observed due to Ca decoration, and carbonization of water hyacinth led to the occurrence of cracks, contributing to the increase in adsorption capacity and rate. Pseudo-second-order model fitted well to the adsorption process. Formation of acicular $\text{Ca}_5(\text{PO}_4)_3\text{OH}$ nanoparticles contributed to the favorable adsorption process. Therefore, this work provides a new insight into conversion of sludge and water hyacinth into adsorbent in application of phosphorus pollution remediation.

Materials and Methods

Materials. Water hyacinth (W) was collected from the Pear River in Guangzhou, further being dried and ground into powder less than 100 meshes. The volatile content was 77.47%. Dewatered sewage sludge was collected from Lijiao sewage treatment plant, in Guangzhou, China, and subsequently being dried by an oven set at 105°C . Table S1 showed that the volatile of dried sludge was 31.47%. C, O, Al, Si, Fe were the main elements in dried sludge. Also, Ca and P were also observed in the initial dried sludge. The ash mass content of the dried sludge is high to 48.54%. Calcium carbonate (CaCO_3) and potassium phosphate (K_3PO_4) were chemical grade purchased from sigma reagent Corporation, USA.

Preparation of adsorbent. Ca-decorated biochar was prepared by carbonization in a programmable tube furnace at 800°C . Firstly, the sludge was mixed with CaCO_3 and water hyacinth in a mass ratio of 1:1, being carbonized at 800°C in a tube furnace (SKF-210, Hangzhou Lantian Instrument Co., China) and washed by deionized water to remove the residual ions. The obtained sample was named as S-Ca-11 according to the mass ratio of sludge to CaCO_3 was 1:1. In addition, the sludge, water hyacinth and CaCO_3 were mixed in varied mass ratio to investigate the effect of each component on the adsorption behavior. These samples were prepared as described above. These resulted samples were named as SW-Ca-112, SW-Ca-325, SW-Ca-415, SW-Ca-221, SW-Ca-441 according to the mass ratio of sludge, water hyacinth and CaCO_3 were 1:1:2, 3:2:5, 4:1:5, 2:2:1, 4:4:1, respectively.

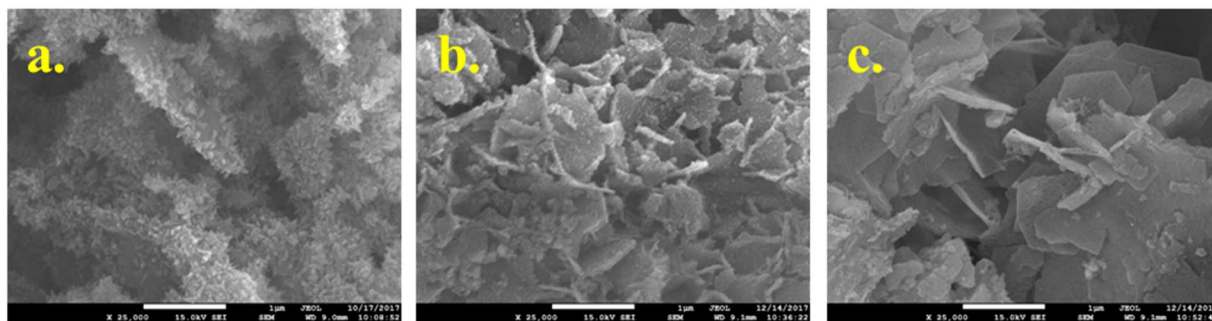


Figure 6. SEM morphologies of (a) SW-Ca-112, (b) SW-Ca-325 and (c) SW-Ca-415 after adsorption of P.

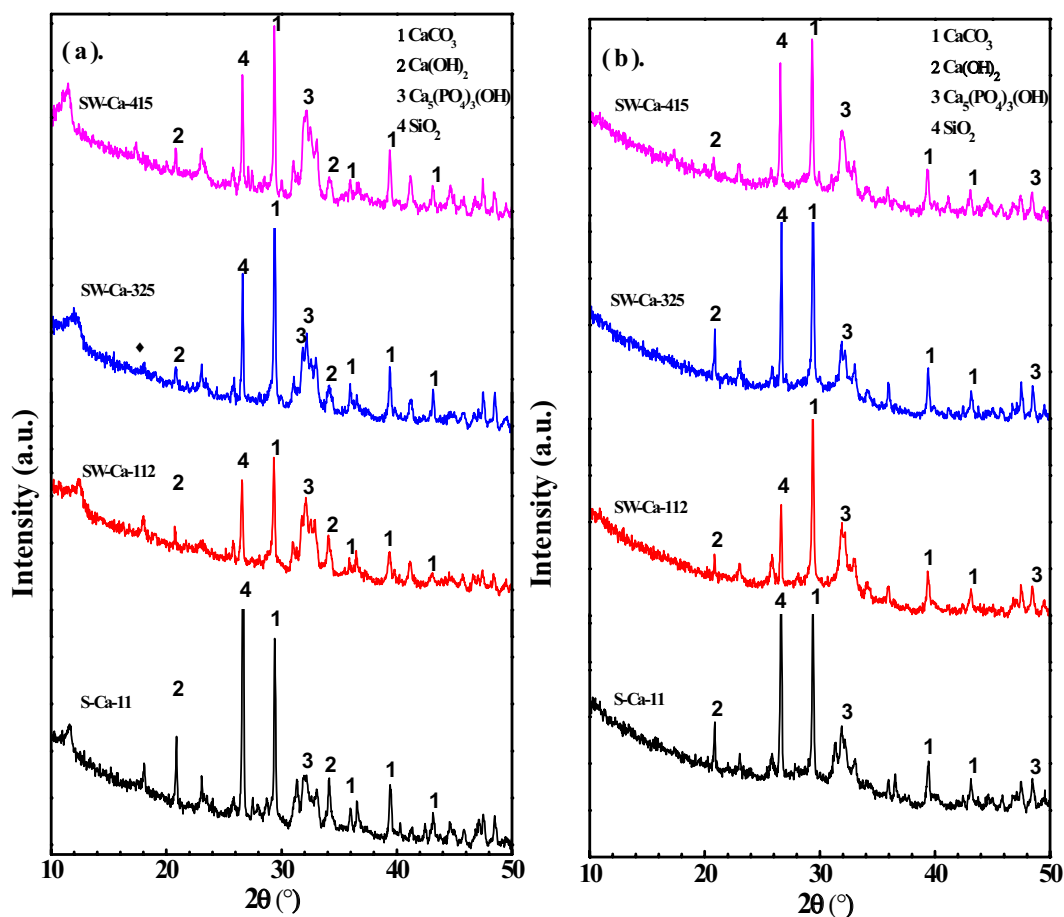


Figure 7. XRD patterns of the sludge derived biochars in the presence of Ca and water hyacinth (a) before adsorption, (b) after adsorption.

Sample	C	O	Mg	Al	Si	P	K	Ca	Fe
SW-Ca-112	28.84	41.01	0.66	0.68	2.49	5.91	0.26	18.9	1.25
SW-Ca-415	11.52	45.51	0.6	1.41	3.03	6.93	0.28	28.73	1.98
SW-Ca-325	15.57	44.82	0.62	1.04	2.64	8.46	0.4	24.58	1.88
S-Ca-11	14.81	44.46	0.46	1.76	4.24	7.62	0.52	23.93	2.2

Table 4. EDS analysis results (wt%) of the sludge derived biochars in the presence of various ratios of sludge to Ca and water hyacinth after P adsorption.

Adsorption experiments. A stock solution containing 1,000 mg/L P was prepared by dissolving K_3PO_4 in deionized water, and the desired solutions were prepared by diluting the stock solution. In the adsorption experiments, the adsorbent dose was 1.000 g/L. All concentrations are expressed in $P-PO_4^{3-}$. All batch adsorption experiments were performed in conical flasks with a plug on a shaker equipped with a thermostat at 200 rpm and at 25 °C.

Adsorption kinetic was investigated by conducting an initial P concentration of 50 mg/L, and the residual sample at each determined time interval was drawn. For each test, the suspension was filtrated through a 0.45 μ m cellulose acetate membrane, and the residual P concentration in the filtrate was measured using an ultraviolet spectrophotometer at 700 nm (HITACHI U-2910, Japan). The adsorption amount was calculated as the difference between the initial and residual concentrations.

All experiments were repeated thrice, and the average value was calculated. The adsorption capacities at different time t (q_t , mg/g) were calculated as follows:

$$q_t = \frac{(C_0 - C_t)V}{m} \quad (1)$$

where C_0 and C_t (mg/L) represent the P concentration at initial and t time (min), respectively. V (L) represents the volume of the solution, and m (g) represents the adsorbent mass.

Adsorption kinetic models. To further understand the effect of the addition of Ca and water hyacinth on the adsorption behavior of P, two widely used pseudo-first-order and pseudo-second-order kinetic models were linear fitted as shown below to describe the adsorption kinetics⁴⁰.

$$\ln(q_e - q_t) = \ln q_e - k_1 t \quad (2)$$

$$\frac{t}{q_t} = \frac{1}{k_2 q_e^2} + \frac{t}{q_e} \quad (3)$$

where q_t and q_e (mg/g) represented the adsorption amounts of phosphorus at t time and equilibrium, respectively. t (min) represents the adsorption time. k_1 , k_2 were the adsorption rate constants of pseudo-first-order model, pseudo-second-order kinetic model, respectively.

Analytical method. The major phase of biochar before and after adsorption of PO_4^{3-} were characterized through XRD analysis using a D/max 2200 vpc diffractometer (Rigaku Corporation, Japan) with Cu $K\alpha$ radiation at 40 kV and 30 mA, to investigate their transformation behaviors and fates. Scanning electron microscopy (SEM) images were observed using a JEOL JSM-6330F-mode Field Emission Scanning Electron Microscope (JED-2300).

References

- Cordell, D., Drangert, J.-O. & White, S. The story of phosphorus: global food security and food for thought. *Global Environ. Change* **19**, 292–305 (2009).
- Cooper, J., Lombardi, R., Boardman, D. & Carliell-Marquet, C. The future distribution and production of global phosphate rock reserves. *Resour. Conserv. Recycl.* **57**, 78–86 (2011).
- Koilraj, P. & Sasaki, K. Selective removal of phosphate using La-porous carbon composites from aqueous solutions: batch and column studies. *Chem. Eng. J.* **317**, 1059–1068 (2017).
- Li, R. *et al.* Enhancing phosphate adsorption by Mg/Al layered double hydroxide functionalized biochar with different Mg/Al ratios. *Sci. Total Environ.* **559**, 121–129 (2016).
- Li, R. *et al.* Recovery of phosphate from aqueous solution by magnesium oxide decorated magnetic biochar and its potential as phosphate-based fertilizer substitute. *Bioresour. Technol.* **215**, 209–214 (2016).
- Lim, B. H. & Kim, D.-J. Selective acidic elution of Ca from sewage sludge ash for phosphorus recovery under pH control. *J. Ind. Eng. Chem.* **46**, 62–67 (2017).
- Liu, H., Sun, X., Yin, C. & Hu, C. Removal of phosphate by mesoporous ZrO_2 . *J. Hazard. Mater.* **151**, 616–622 (2008).
- Liu, J., Zhou, Q., Chen, J., Zhang, L. & Chang, N. Phosphate adsorption on hydroxyleironelanthanum doped activated carbon fiber. *Chem. Eng. J.* **215–216**, 859–867 (2013).
- Lin, J. *et al.* Effect of calcium ion on phosphate adsorption onto hydrous zirconium oxide. *Chem. Eng. J.* **309**, 118–129 (2017).
- Kelessidis, A. & Stasinakis, A. S. Comparative study of the methods used for treatment and final disposal of sewage sludge in European countries. *Waste Manag.* **32**, 1186–1195 (2012).
- Pradel, M., Aissani, L., Villot, J., Baudez, J. C. & Laforest, V. From waste to added value product: towards a paradigm shift in life cycle assessment applied to wastewater sludge: a review. *J. Clean. Prod.* **131**, 60–75 (2016).
- Li, N., Wei, D., Wang, S., Hu, L. & Xu, W. Comparative study of the role of extracellular polymeric substances in biosorption of Ni(II) onto aerobic/anaerobic granular sludge. *J. Colloid Interf. Sci.* **490**, 754–761 (2017).
- Li, W. H., Yue, Q. Y., Gao, B. Y., Ma, Z. H. & Li, Y. J. Preparation and utilization of sludge-based activated carbon for the adsorption of dyes from aqueous solutions. *Chem. Eng. J.* **171**, 320–327 (2017).
- Li, J. S. *et al.* Change in re-use value of incinerated sewage sludge ash due to chemical extraction of phosphorus. *Waste Manag.* <https://doi.org/10.1016/j.wasman.2018.01.007> (2018).
- Smith, K. M., Fowler, G. D., Pullket, S. & Graham, N. J. Sewage sludge-based adsorbents: A review of their production, properties and use in water treatment applications. *Water Res.* **43**, 2569–2594 (2009).
- Jaria, G., Calisto, V., Gil, M. V., Otero, M. & Esteves, V. I. Removal of fluoxetine from water by adsorbent materials produced from paper mill sludge. *J. Colloid Interf. Sci.* **448**, 32–40 (2015).
- Li, W. H., Yue, Q. Y., Gao, B. Y., Wang, X. J. & Qi, Y. F. Preparation of sludge-based activated carbon made from paper mill sewage sludge by steam activation for dye wastewater treatment. *Desalination.* **278**, 179–185 (2011).
- Xiao, B., Dai, Q., Yu, X., Yu, P. & Zhai, S. Effects of sludge thermal-alkaline pretreatment on cationic red X-GRL adsorption onto pyrolysis biochar of sewage sludge. *J. Hazard. Mater.* **343**, 347–355 (2017).
- Chen, Y. D., Ho, S. H., Wang, D., Wei, Z. S. & Chang, J. S. Lead removal by a magnetic biochar derived from persulfate-ZVI treated sludge together with one-pot pyrolysis. *Bioresour. Technol.* **247**, 463–470 (2017).

20. Bandosz, T. J. & Block, K. Municipal sludge-industrial sludge composite desulfurization adsorbents: synergy enhancing the catalytic properties. *Environ. Sci. Technol.* **40**, 3378–3383 (2006).
21. Kong, L. J. *et al.* Conversion of Fe-rich waste sludge into nano-flake Fe-SC hybrid Fenton-like catalyst for degradation of AOII. *Environ. Pollut.* **216**, 568–574 (2016).
22. Lebigue, C. J., Andriantsiferana, C., Krou, N., Ayrat, C. & Mohamed, E. Application of sludge-based carbonaceous materials in a hybrid water treatment process based on adsorption and catalytic wet air oxidation. *J. Environ. Manag.* **91**, 2432–2439 (2010).
23. Marques, R. R. N., Stüber, F., Smith, K. M., Fabregat, A. & Bengoa, C. Sewage sludge based catalysts for catalytic wet air oxidation of phenol: Preparation, characterisation and catalytic performance. *Appl. Catal. B. Environ.* **101**, 306–316 (2011).
24. Tu, Y. T., Tian, S. H., Kong, L. J. & Xiong, Y. Co-catalytic effect of sewage sludge-derived char as the support of Fenton-like catalyst. *Chem. Eng. J.* **185**, 44–51 (2012).
25. Adam, C., Peplinski, B., Michaelis, M., Kley, G. & Simon, F. G. Thermochemical treatment of sewage sludge ashes for phosphorus recovery. *Waste Manag.* **29**, 1122–1128 (2009).
26. Kong, L. J. *et al.* Nano-rod Ca-decorated sludge derived carbon for removal of phosphorus. *Environ. Pollut.* **233**, 698–705 (2018).
27. Arenas, E. & Chejne, F. The effect of the activating agent and temperature on the porosity development of physically activated coal chars. *Carbon* **42**, 2451–2455 (2004).
28. Ioannidou, O. & Zabaniotou, A. Agricultural residues as precursors for activated carbon production-A review. *Renew. Sust. Energ. Rev.* **11**, 1966–2005 (2007).
29. Li, Y., Li, Y., Li, L., Shi, X. & Wang, Z. Preparation and analysis of activated carbon from sewage sludge and corn stalk. *Adv. Pow. Technol.* **27**, 684–691 (2016).
30. Wu, C., Song, M., Jin, B., Wu, Y. & Huang, Y. Effect of biomass addition on the surface and adsorption characterization of carbon-based adsorbents from sewage sludge. *J. Environ. Sci.* **25**, 405–412 (2013).
31. Malik, A. Environmental challenge vis a vis opportunity: The case of water hyacinth. *Environ. Int.* **33**, 122–138 (2007).
32. Santibañez-Aguilar, J. E., Ponce-Ortega, J. M., González-Campos, J. B., Serna-González, M. & El-Halwagi, M. M. Synthesis of Distributed Biorefining Networks for the Value-Added Processing of Water Hyacinth. *ACS Sustain. Chem. Eng.* **1**, 284–305 (2013).
33. Phothisantikul, P. P., Tuanpusa, R., Nakashima, M., Charinpanitkul, T. & Matsumura, Y. Effect of CH₃COOH and K₂CO₃ on Hydrothermal Pretreatment of Water Hyacinth (*Eichhorniacrassipes*). *Ind. Eng. Chem. Res.* **52**, 5009–5015 (2013).
34. Wang, S. D. *et al.* Adsorption of phosphorus by calcium-flour biochar: Isotherm, kinetic and transformation studies. *Chemosphere* **195**, 666–672 (2018).
35. Tran, H. N., You, S. J., Hosseinbandegharai, A. & Chao, H. P. Mistakes and inconsistencies regarding adsorption of contaminants from aqueous solutions: A critical review. *Water Res.* **120**, 88–116 (2017).
36. Mitrogiannis, D. *et al.* Removal of phosphate from aqueous solutions by adsorption on to Ca(OH)₂ treated natural clinoptilolite. *Chem. Eng. J.* **320**, 510–522 (2017).
37. Kilpimaa, S., Runtti, H., Kangas, T., Lassi, U. & Kuokkanen, T. Physical activation of carbon residue from biomass gasification: Novel sorbent for the removal of phosphates and nitrates from aqueous solution. *J. Ind. Eng. Chem.* **21**, 1354–1364 (2015).
38. Lin, J. *et al.* Effect of calcium ion on phosphate adsorption onto hydrous zirconium oxide. *Chem. Eng. J.* **309**, 118–129 (2017).
39. Ren, Z., Shao, L. & Zhang, G. Adsorption of Phosphate from Aqueous Solution Using an Iron-Zirconium Binary Oxide Sorbent. *Water. Air. Soil. Pollut.* **223**, 4221–4231 (2012).
40. Wang, D., Chen, N., Yu, Y., Hu, W. & Feng, C. Investigation on the adsorption of phosphorus by Fe-loaded ceramic adsorbent. *J. Colloid. Interf. Sci.* **464**, 277–284 (2016).

Acknowledgements

This research was supported by the National Nature Science Foundations of China (Nos 51508116, 21407155, U1501231), the Nature Science Foundations of Guangdong Province (2016A030310265), the Science and Technology Research Programs of Guangzhou City (201607010311), Guangzhou University's 2017 training program for young top-notch personnels (BJ201706), the Project of Guangdong Provincial Key Laboratory of radioactive contamination control and resources (2012A061400023), the Hongkong Scholarship (XJ2016037).

Author Contributions

L.J. Kong prepared all the Figures and writes the manuscript, X. Hu, Z. Xie and X. Ren conducted the experiments, D.Y. Chen and J. Long analysis the results, K. Shih, M.H. Su, Z.H. Diao, L. Hou provides suggestion. All authors reviewed the manuscript and agreed to submit the manuscript.

Additional Information

Supplementary information accompanies this paper at <https://doi.org/10.1038/s41598-018-31750-6>.

Competing Interests: The authors declare no competing interests.

Publisher's note: Springer Nature remains neutral with regard to jurisdictional claims in published maps and institutional affiliations.



Open Access This article is licensed under a Creative Commons Attribution 4.0 International License, which permits use, sharing, adaptation, distribution and reproduction in any medium or format, as long as you give appropriate credit to the original author(s) and the source, provide a link to the Creative Commons license, and indicate if changes were made. The images or other third party material in this article are included in the article's Creative Commons license, unless indicated otherwise in a credit line to the material. If material is not included in the article's Creative Commons license and your intended use is not permitted by statutory regulation or exceeds the permitted use, you will need to obtain permission directly from the copyright holder. To view a copy of this license, visit <http://creativecommons.org/licenses/by/4.0/>.

© The Author(s) 2018